Comparison of dynamic and static backface deformation measures

K. Loftis[1], D. Barnes[2]

[1]*Army Futures Command, DEVCOM Analysis Center, Aberdeen Proving Ground, MD, USA, (kathryn.l.loftis2.civ@army.mil)*
[2]*Survice Engineering, Aberdeen, MD*

Abstract. The development of a medically-based behind-armour blunt trauma (BABT) injury criterion for evaluation of body armour (BA) performance remains a top priority for the U.S. Army and may lead to improved specifications and requirements for non-perforating BA impacts. Further, an updated criterion may open the design space for new materials and designs. This study investigated the backface dynamics and static residual deformation of hard plates impacted ballistically without complete penetration. High-speed video analysis of twelve gelatin-backed plate ballistics tests was used to characterise the dynamic backface response, and computed tomography (CT) analysis of the impacted plates were performed to obtain measurements of the static residual deformations. Hard plates with only a single curvature were used for this initial study to allow visualization of the backface deformation in a single view on high-speed camera and geometric (depth and area) and rate measurements were recorded. Further, a secondary backface deformation phenomenon was observed in high-speed video and compared to the dynamic deformation. Before and after the tests, the plates were CT scanned and analysis of static deformations was completed. Static backface deformations varied from 7.4 to 10.3 mm and maximum dynamic deformations varied from 29.7 to 38.0 mm. The secondary backface deformation observed in high-speed video varied from 4.1 to 13.7 mm. In this study, the static backface deformation did not correspond to the maximum dynamic backface deformation. The contradiction between static and dynamic backface deformation indicates that using static deformation as the sole indicator of BABT is insufficient. The observed secondary backface deformation was more consistent with the static measurements than dynamic. There was also a difference seen in deformation rates between initial backface deformations and maximum backface deformations. Additional testing and continued analysis should be conducted to gain more information regarding pertinent metrics for BABT injury risk.

1. INTRODUCTION

Current performance requirements for Army body armour are only loosely correlated to injury. The development of a medically based behind-armour blunt trauma (BABT) injury criterion for use as the basis for body armour performance requirements remains a top priority. Developing an injury criterion that can be used to develop specifications and requirements associated with non-perforating body armour impacts will significantly improve evaluation capabilities of military body armour. Previous experimental tests performed by multiple groups have investigated the loading characteristics behind armour, but it is currently unknown whether dynamic measures of deformation are related to static measures of deformation after an impact event (1-14). When analyzing body armour from real-world events, it is not possible to measure dynamic deformations, so it is currently unknown how well static measurements relate to BABT injury (15-17). Additionally, previous research has shown that backed materials deform differently than unbacked materials, which makes viewing and measurement of dynamic deformations more difficult than static measures. The goal of this article was to investigate static and dynamic measures of backed protective plates to understand if the two could be correlated for future behind armour blunt trauma studies.

2. METHODS

A hard plate was placed against a 20% gel block with a molded face so that the plate fit up against the gel with no gap or spacing. Both ends of the gel block were molded so that gel blocks could be used for two different tests (by turning it around for the second shot). No soft armour was used, as that would have prevented viewing of the full backface deformation. The test setup included two high-speed cameras orthogonal to the plate to capture pitch and yaw of the threat at impact, as well as capturing backface deformation shape and velocity on the back of the plate. Gel blocks were back-lit with diffused light banks to eliminate glare and intense regions of light to get clear views to measure backface deformation and velocity. Video frame rates were set at 80,000 frames per second (fps) to maintain appropriate field of view and image resolution while capturing the dynamic features of the test.

https://doi.org/10.52202/080042-0012

Twelve plates were tested in two cycles using two different threats (Table 1). A universal receiver gun was used to launch the threat, and the powder in the threat was hand-loaded to target the desired velocity. The prescribed threat velocity at impact was the same for both threats. Threats are listed as A or B, with A being the first one tested. All plates were pre- and post-scanned via computed tomography (CT). A preliminary analysis of the results was performed during the pause in testing to determine if any adjustments should be made. Following this review, it was determined that the results were as expected, so testing for round two was completed with the same setup and parameters as round one. Postshot analysis consisted of two unique methods for measuring static and dynamic backface deformation. Each method will be presented separately, with a comparison of the final results. A blind analysis of the postshot data was conducted so that results were not biased by the analysts.

Table 1. Test matrix for plates on gelatin

Threat	Tests
A	1, 2, 3
B	4, 5, 6
A	7, 8, 9
B	10, 11, 12

2.1 Residual Static Backface Deformation Measurement Method

Each plate was CT-scanned before and after testing. A standard protocol developed by DEVCOM Analysis Center was used, which includes scanning without extended Hounsfield units, with the plate lying on the CT bed and a radiographic grid behind the plate for reference. Preshot CT analysis, using the CT scout X-ray (XR), verified that the plates were undamaged and did not contain any defects prior to testing. Postshot CT analysis included determining the location of the centre of impact, and measuring overall plate thickness, maximum static deformation, and the radius of the extent of hard damage. All CT analysis was completed in Mimics version 23 (Materialize NV, Leuven, Belgium), with calculations completed in Excel 2016 (Microsoft, Redmond, WA). The method was adapted from previous plate analysis (15-17). For definition of the coordinate space for each plate, the top, bottom, left, and right corners were chosen and x, y, z coordinates were recorded. Using the coronal view from CT, the outermost slice showing the hard damage was chosen. Then a circle was defined around the hard damage using the 3-point method, as shown in Figure 1. The centre of this circle was then used to define the centre of damage for reference points from which maximum deformation and undeformed thickness were measured (B). This is possible with CT because the three views (axial, coronal, and sagittal) are linked. So, to gather the coordinates of the estimated undeformed front/back of the plate at the site of maximum deformation, the sagittal view was adjusted until the circle centre was in view. Then where the line between the top and bottom of the plate of the front surface within that view was intersected by the line along the maximum damage was chosen as the estimated undeformed plate front point (A). The same was repeated for recording the estimated undeformed plate back point (C). Along the same line, the maximum point of deformation was also recorded (D). The linear measurements were then computed using the distance formula between each set of points using the x, y, z, coordinates.

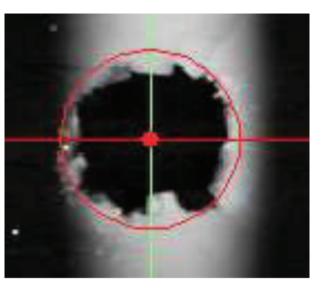

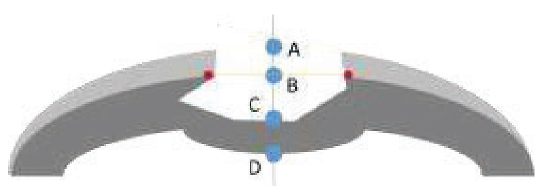

Figure 1. (left) Example coronal CT image of circle defining the damage in the plate, (right) Axial slice example diagram showing measurement points: A undamaged surface point, B internal damage centre, C undamaged back point, D maximum static deformation, where the yellow line defines the front plane of hard damage and the green line defines the centre of hard damage.

https://doi.org/10.52202/080042-0012

2.2 High-Speed Video Dynamic Backface Analysis Method

High-speed video was collected by two cameras (Photron FASTCAM SA4 model 500K-M3E), overhead and side views, aligned orthogonal to the gelatin block. The overhead-view camera focused on the superior surface of the plate while a side-view camera focused on the left lateral surface of the plate. Each camera was aligned such that the centre of the camera view was at the centre of the respective plate surfaces. The overhead-view camera used a Canon EF 50-mm lens with an f-stop of 9.9 and focus set at 3800 mm. The side-view camera used a Canon zoom EF 28–135-mm lens with an f-stop of 4.9 and focus set at 1100 mm. The lenses were controlled by Birger Engineering Interface software (v1.1.9). The frame rate and shutter speed of the cameras were set to 80,000 fps and 1/177,000 s, respectively, for all tests, with the exception of test one for which a frame rate and shutter speed of 72,000 fps and 1/98,000 s were used. Given these frame rates, the maximum resolution for each high-speed video was 192 × 192 pixels, with a viewing area of approximately 180 ×180 mm.

The viewing area was sufficient to capture the threat prior to contact with the plate as well as the full extent of backface deformation throughout the event. Two light banks comprised of 42 ERV halogen lamps, each rated at 340 W, were used to backlight the plate and gelatin during testing. High-speed video was captured for 0.5 s and was triggered in sync with the universal receiver. Prior to testing, a grid scale composed of white and black 1- by 1-inch squares was placed in each camera view and a single image was captured for determination of pixel dimensions.

Each high-speed video was exported as a TIF file. The TIFs were imported into MATLAB (version R2021a, Mathworks, MA, USA) for postprocessing and calculation of backface deformation metrics. Initially, the grid scale image was opened and viewed using the “imread” and “image” functions (Figure 2). The “colormap” function was used to apply a 256-bit gray scale to the grid image and each pixel was assigned a gray scale index value. The difference in index value between the white and black squares of the grid was used to measure the size of each grid square in both the vertical and horizontal axes of the image. Transitions between white and black were determined over 40 rows of pixels (horizontal direction of view) and 180 columns of pixels (vertical direction of view), and the average number of pixels between transitions formed the number of pixels-per-inch along the two axes (horizontal and vertical). The measurements were then converted from pixels-per-inch to pixels-per-millimeter and recorded for calculation of backface deformation.

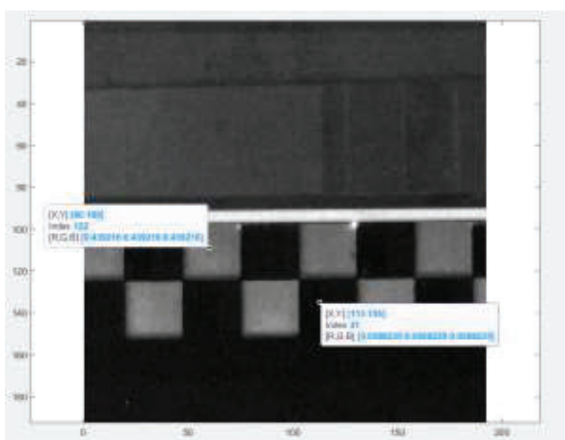

Figure 2. Gray-scale grid-scale image with the index of a pixel within a white square (index value 122) and index pixel within a black square (index value 31)

Next, a TIF displaying the threat during approach toward the front of the plate was opened and viewed in a similar manner as the image of the grid scale. The colourmap function was again used to apply a 256-bit gray scale to the image. With backlighting, the transition between solid material (i.e., the plate) and gel or air was a pixel index of 256, where the solid material is associated with a pixel index below 256, while gel and/or air had an associated pixel index greater than 256. The indexes were then used to determine the pixel location (row and column) of the rearmost portion of the plate along the shot line. This pixel was used as an initial origin for backface deformation during video analysis.

Finally, each TIF image of the high-speed video was opened using the imread function and a 192 × 192 matrix of gray scale pixel indices was created for each frame using the impixel function. These matrices were created for the first 200 frames of the video, as this sufficiently captured the full backface deformation. Comparison of the indices’ values between the first frame and subsequent 199 frames were performed to identify pixels that were initially above an index value of 225 (gelatin) in the first frame and changed to an index value below 225 (plate) in subsequent frames. These changed pixels were assigned a "1" while all other pixels were assigned a "0". From this comparison, a second set of 199 binary matrices of 0s and 1s was created. An index value of 225 was chosen for this portion of the analysis because, although an index of 256 provided a clear distinction between solid material (the plate) and gelatin prior to initiation of backface deformation, it was observed that the gray scale index value of compressed gelatin fell slightly below 256. Therefore, to be certain that the backface deformation was accurately tracked as it compressed the gelatin, the threshold between the backface and gelatin was set at a pixel index value of 225. Inspection of initial frames of the video, prior to deformation occurring, indicated that using an index of 225 rather than 256 reduced the plate depth by only one pixel, if any, at any point along the backface.

2.3 Calculation of Dynamic Backface Deformation Metrics

The binary matrices from the overhead view camera were used to quantify geometric and rate-based metrics associated with dynamic backface deformation. The metrics calculated were depth of deformation, rate of deformation, area of deformation, and rate of change of the area of deformation (Table 2). Depth of deformation and rate of deformation were measureable along any desired vector extending posterior from the initial point of backface deformation. For this study, the apex of the backface deformation was identified frame by frame. Thus the maximum depth of deformation was measured over time, rather than assuming a set vector along which the metrics were measured. Figure 3 depicts an example video frame of backface deformation with the depth of deformation and area of deformation metrics highlighted. The rate of deformation was initially calculated on a frame-by-frame basis, where the rate for a given frame was the change in deformation from the prior frame, divided by the inverse of the video frame rate. The frame-by-frame deformation rate was observed to be highly variable, particularly as the rate of deformation decreased with increased depth. This variability is likely due limited resolution provided the high frame-rate requirements needed to capture initial deformation. Therefore, a moving average technique was used, which smoothed the frame-by-frame deformation rate by averaging each frame-by-frame rate with the prior and subsequent rates. Side-view camera videos were used to confirm the shape of the backface deformation but were not used for calculation of deformation metrics.

Table 2. Backface deformation metrics measured from analysis of high-speed video

Metric	Description	Units
Depth of deformation	Number of pixels identified as having transitioned from gelatin to backface along the apex of deformation (assigned "1" in the binary matrix), converted according to the grid scale measurements.	mm
Rate of deformation	Frame-by-frame change in depth of deformation divided by the video frame rate. The rate of deformation is smoothed by averaging the frame-by-frame rate with one prior frame and one subsequent frame.	mm/s
Area of deformation	Total number of pixels identified as having transitioned from gelatin to backface ("1" in the binary matrix) in the plane of the video, converted to area according to the grid scale measurements. Area of deformation does not represent a surface area of deformation, but rather a 2-D measurement of the area of the deformation within that specific plane.	mm^2
Rate of change of area of deformation	Frame-by-frame change in area of deformation within the transverse plane of the plate divided by the video frame rate. The rate of area of deformation is smoothed by averaging the frame-by-frame rate with one prior frame and one subsequent frame.	mm^2/s

https://doi.org/10.52202/080042-0012

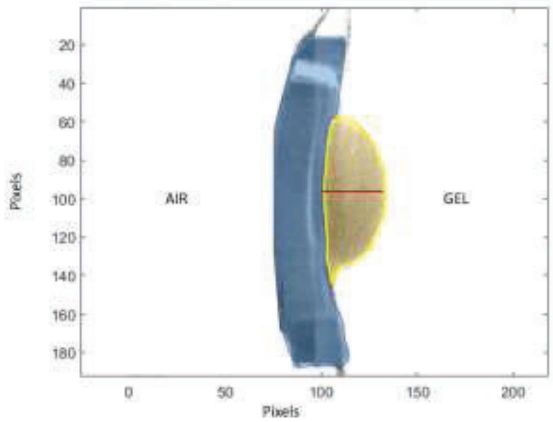

Figure 3. Exemplar high-speed video frame of dynamic backface deformation. The exemplar plate is represented in blue. The red line indicates the maximum depth of deformation while the total area of deformation is highlighted in yellow. For releasability, the front damage profile has been removed from the image.

2.4 Secondary Deformation Phenomenon from High-speed Video

Review of the overhead view high-speed video indicated that following the primary backface deformation, the backface appeared to return to its original form, and then deform again near the culmination of the video. Thus, a methodology was developed to quantify the observed secondary deformation phenomenon. Similar to the dynamic analysis, the imread function was utilised to import individual TIF files into Matlab. Once imported, the pixel values were utilised to manually identify the depth of the superior surface of the plate at two locations: (1) the point of threat impact (i.e. shot line) and (2) the right end of the plate. The former depth was utilised to identify static deformation of the backface relative to the initial depth of the plate along the shotline. The latter depth was utilised to aid in identifying change in the location of the superior surface of the plate within the camera view as the plate compressed the gelatin surface. This analysis was performed at increments of 250 frames from the first to final high-speed video frames. Once the potential plate shift was accounted for, backface deformation was identified in the final three incrementally-chosen frames and normalised to threat velocity. The prior frames were used to ensure that the depth of the superior surface of the plate was identifiable throughout the test.

3. RESULTS

All 12 plate tests on gelatin were completed successfully. Although threats A and B were meant to be striking the target at the same velocity, due to small variations in testing, threat A velocities were slightly lower than the overall mean while threat B were higher than the mean. For this reason, the results are presented as normalised according to incoming threat velocity, but due to releasability restrictions, actual velocities are not presented here. Of note however, the range in velocities overall was less than 16 m/s. To complete the normalization, all velocities were ordered and then normalised relative to the greatest velocity. A normalisation factor of 1.0 was assigned to that greatest velocity ($V_{greatest}$), while all other velocities (v_i) were assigned a normalisation factor (NF_i) greater than 1.0, according to Equation 1. Pertinent static and dynamic measurements were normalised based on these normalization factors.

$$NF_i = \frac{V_{greatest}}{V_i} \tag{1}$$

3.1 CT Static Deformation

For the static residual methodology, each plate was examined manually using Hounsfield unit values in the axial, coronal, and sagittal views of the postshot CT scan, with 3-D representation only used for visualization purposes. Figure 1 shows an example of the 3-D representation from CT and a view showing the coordinate points gathered.

A summary of the static residual plate deformation measurements is shown in Table 3. All results shown are normalised by threat velocity. The static postshot deformation was determined by subtracting

https://doi.org/10.52202/080042-0012

the plate back surface of the post-impact plate from the back surface original plate at the impact location. To indicate the degree of plate damage, the postshot radius of damage was measured. This measurement was defined by fitting a circle around the damage within the plate and obtaining its radius. Results showed a statistically significant difference between the two sets of damage results, with the first set (A) having larger linear backface deformations but smaller radius of damage compared to set B.

Table 3. Static residual plate deformation measurements from CT

Test ID	Velocity Normalisation Factor	Normalised Post-shot Deformation (mm)	Normalised Post-shot Damage Radius (mm)
1 A	1.004	8.93	15.76
2 A	1.012	8.83	15.93
3 A	1.012	8.69	16.49
7 A	1.020	9.98	18.89
8 A	1.019	9.77	17.00
9 A	1.025	10.30	16.72
4 B	1.017	7.42	16.87
5 B	1.004	7.56	17.25
6 B	1.001	9.44	19.27
10 B	1.000	9.19	20.21
11 B	1.010	7.64	18.57
12 B	1.004	7.86	22.81
Total mean (SD)	NA	8.79 (0.99)	17.98 (2.06)
Mean (SD), A, B	NA	9.41 (0.68), 8.18 (0.89)	16.79 (1.13), 19.16 (2.17)
T-test (A vs B)	NA	$p = 0.045$	$p = 0.029$

3.2 High-Speed Video Analysis of Dynamic Deformation

Geometric and rate-based metrics were normalised and differences in metrics between threat types were determined using student t-tests (Tables 4 and 5). The maximum normalised depth of deformation varied from 29.7 to 38.0 mm with a mean of 32.2 mm for all tests (Table 4). The maximum depth of deformation tended to be greater for threat B than for threat A, but the difference in means was not significant ($p = 0.055$). The time of maximum depth, relative to initiation of deformation, varied from 1.31 to 1.75 ms with a mean of 1.56 ms for all tests. Maximum depth of deformation occurred in significantly less time for threat B than for threat A ($p = 0.001$). The area of deformation at maximum depth varied from 1898 to 2579 mm² with a mean of 2267 mm² for all tests. The area of deformation at maximum depth was not significantly different between threats A and B ($p = 0.481$).

https://doi.org/10.52202/080042-0012

Table 4. Backface deformation depth and area measurements normalised to threat velocity. Time of maximum depth was not normalised.

Test ID	Maximum Depth (mm)	Time of Maximum Depth (ms)	Deformation Area at Maximum Depth (mm²)
1 A	31.7	1.75	2515
2 A	31.6	1.63	2282
3 A	29.7	1.64	2330
7 A	30.7	1.60	2036
8 A	29.7	1.63	2061
9 A	31.8	1.68	2069
4 B	32.6	1.41	2579
5 B	32.2	1.54	2556
6 B	30.3	1.46	2277
10 B	35.7	1.31	2077
11 B	38.0	1.56	2520
12 B	32.0	1.49	1898
Mean (SD), A, B	30.8 (1.0), 33.5 (2.8)	1.66 (0.05), 1.46 (0.09)	2216 (192), 2318 (284)
Student t-test	$p = 0.055$	$p = 0.001$	$p = 0.481$

Table 5. Rate of change of backface deformation measurements normalised to threat velocity

Test ID	Maximum Depth Rate (mm/ms)	Time of Maximum Depth Rate (ms)	Maximum Area Rate (mm²/ms)	Time of Maximum Area Rate (ms)
1 A	205	0.014	4175	0.069
2 A	154	0.013	3800	0.063
3 A	103	0.025	3422	0.050
7 A	104	0.025	4739	0.038
8 A	103	0.038	3302	0.038
9 A	104	0.025	3272	0.050
4 B	129	0.038	4317	0.050
5 B	153	0.013	5174	0.063
6 B	102	0.038	3572	0.050
10 B	152	0.013	4431	0.050
11 B	154	0.013	4861	0.050
12 B	229	0.013	4353	0.038
Mean (SD), A, B	129 (43), 153 (42)	0.023 (0.009), 0.021 (0.013)	3785 (581), 4451 (546)	0.051 (0.013), 0.050 (0.008)
T-test	$p = 0.345$	$p = 0.763$	$p = 0.068$	$p = 0.852$

The maximum rate of change in deformation depth varied from 102 to 229 mm/ms with a mean of 141 mm/ms for all tests (Table 5). The maximum rate of change in deformation depth was not significantly different for threats A and B ($p = 0.345$). The maximum rate of change in the deformation area varied from 3272 to 5174 mm²/ms with a mean of 4118 mm²/ms for all tests. The maximum rate of change in deformation area tended to be greater for threat B than for threat A, although the difference between threats was not significant ($p = 0.068$). For each test, the depth rate maximum occurred within two to three frames after initiation of deformation, with the area rate maximum occurring one to two frames following the depth rate maximum. Therefore, the time of the depth rate maxima and area rate maxima did not vary based on threat type ($p = 0.763$ and $p = 0.852$, respectively).

The secondary deformation phenomenon was only observed in video for tests 7 through 12. The duration of high-speed video of tests 1 through 6 was sufficient to properly measure the secondary deformation. The mean depth of the secondary deformation observed in the final 3 frames of the video

https://doi.org/10.52202/080042-0012

analysis are provided in Table 6. Mean secondary deformations were 9.8 mm and 5.7 mm for threats A and B, respectively. A student t-test of the secondary static results found that static deformation was not significantly different between threat types ($p = 0.273$).

Table 6. Secondary residual static deformation measurements from high-speed video for threats A and B normalised to threat velocity, where measurement was possible.

Test ID	Mean Secondary Backface Deformation (mm)
7 A	13.7
8 A	4.1
9 A	11.6
10 B	5.3
11 B	6.6
12 B	5.0
Mean (SD), A, B	9.8 (5.0), 5.7 (0.9)
T-test	p = 0.273

4. DISCUSSION

4.1 CT Analysis of Residual Deformation

The methodology for the CT analysis was developed initially to review returned theatre-damaged plates for BABT deformation and damage, and then relate their damage with injury (or lack thereof). In that scenario, there were no preshot CT scans to compare against. Therefore, for this initial analysis, only the postshot CT scans were used to estimate backface deformation measurements. Yet, in the future it is possible to reevaluate these measurements, comparing the preshot CT of each specific plate with their corresponding postshot CT. Furthermore, a comparison of the two techniques can be performed, including accuracy and ease of calculation. It is important to keep in mind how these measurements are to be used in the future and how applicable the measurement methodologies are in different testing and analysis situations (theatre-event analysis, research, etc.). Work is already in progress to compare these methodologies and expand the analysis.

After review of the CT scans, it should be noted that differences in plate design will result in different BABT characteristics and may also affect the methodology that is best suited for measuring backface deformations. These plates showed very clean, circular damage patterns, making the damage profiling more accurate and repeatable. In visual review of other plate designs with different threats, damage patterns varied greatly, with some resulting in such widespread cracking that this circle methodology would prove difficult. As BABT is investigated for links to injury risk, different plate designs and damage profiles will need to be incorporated to ensure widespread applicability of pertinent metrics.

There was a clear trend in the static deformation measurements from CT. It was possible to perform this analysis on all the plates, as the impacts were focused in the middle of the plates. This methodology would likely need to be revised for edge impacts where it was not possible to centre the damage and easily compare pre and post shot curvature. All plates showed some static deformation upon visual inspection and it was possible to view this deformation via the post-shot CT.

4.2 Video Analysis of Dynamic Deformation

Dynamic backface deformation metrics were successfully calculated from the over-head view camera videos. The curvature of the plates are such that the overhead view captured the depth of backface deformation from initiation to maximum. The full extent of dynamic deformation could not be observed in the side-view camera videos, thus the side-view videos were only used to confirm the rounded shape of the backface deformation. The dynamic backface deformation metrics provided in this study are from a 2-D analysis of the backface response. Therefore, the area of deformation does not represent the area of contact between the backface and the gelatin, but rather the total expansion of the deformed backface within the transverse plane of the plate. Creation of 3-D backface deformation metrics would require additional analysis.

Efforts were made to reduce the effect of parallax in the video analysis. The overhead and side-view cameras were carefully aligned to the centre of the surface of the plate, both vertically and

https://doi.org/10.52202/080042-0012

horizontally, and the cameras were kept orthogonal to the respective plate surfaces. Camera alignment and locations were identical for each test, and alignment of the plate and gelatin were consistent from test to test. When measuring the size of the grid scale (Figure 2), the horizontal lengths of the black and white squares, in pixels, were consistent across the length of the scale. There was no indication of decreased measurement of square size at the edge of the view relative to the centre, indicating limited parallax effect on video measurements. Therefore, any error in measurement of deformation due to parallax was less than that due to the resolution of deformation measurement and consistent from test to test.

The camera frame rate was selected to capture the dynamic nature of the backface deformation while allowing coverage of the entire area of deformation within each camera view with sufficient resolution. The goal of the current study was to create a deformation profile for the entire deformation event. This requires sufficient frame rate to capture high rate changes in deformation early in the event balanced with sufficient resolution to measure small variations in deformation geometry throughout the event. The chosen frame rate of 80,000 fps with a 192 × 192 pixel resolution resulted in a pixel size of approximately 1 mm². This pixel size was sufficient for capturing the geometry of the deformation while allowing for measurement of high rate changes to deformation over time intervals of 0.0125 ms.

4.3 Secondary Deformation Phenomenon from High-speed Video

The secondary backface deformation typically became quantifiable after 2000 high-speed video frames (0.025 seconds) and continued to be observed throughout the remainder of the video (approximately 3000 frames). Further, the depth of the secondary deformation remained consistent for the final video 500-750 frames. As shown in Table 6, the secondary backface deformation has a similar trend as the CT residual static deformation measurements, with greater secondary deformation for threat A than threat B. Thus, the secondary backface phenomenon may be the permanent final deformation observed in the CT analysis. However, this can not be confirmed at this time and further study is required to better understand the secondary deformation phenomenon. Most previous studies of backface deformation do not include data far enough after the event to look for this phenomenon in other testing. For future work, it is strongly advised to record data over a longer time frame to further investigate this finding. The phenomenon is likely material-dependent, so new testing of materials should record longer data to investigate further.

4.4 Comparison of Static and Dynamic Deformation Measurements

Figure 4 depicts the mean dynamic, static, and secondary backface deformations for all tests. Comparison of the results suggests that the generally accepted static CT depth measurements may not adequately describe the dynamic backface response and further investigation of alternative metrics may be warranted. Additionally, the secondary backface deformations more closely followed the trends seen for the static deformations from CT, but given the small number of cases where it was possible to measure this, more research is needed. Results are shown relative to threats A and B to simply show the reversal of maximum deformation between dynamic and static measurements. More research is needed to confirm the results of this small study and investigate a wider range of threats and velocities. Overall, these results show that there is little relationship between static and dynamic measures of deformation and this should be taken into account when investigating metrics for estimating injury from behind-armor effects.

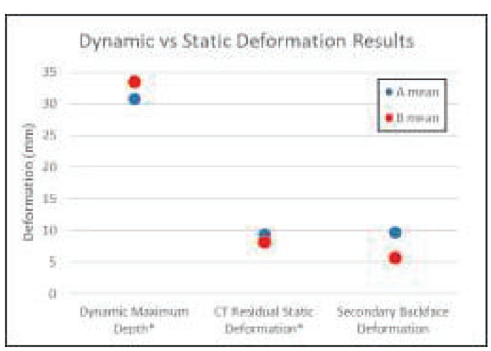

Figure 4. Comparison of dynamic and static deformation measurements for tests normalised to velocity, where * represents comparison results that were statistically significant at the p = 0.05 level.

https://doi.org/10.52202/080042-0012

5. CONCLUSION

The current study found that baseline post-CT hard-plate static deformation measurements trended opposite to the maximum depth of dynamic backface deformation observed in high-speed video. The tests with lesser static deformation had greater depth of dynamic deformation. Further, a secondary backface deformation phenomenon was observed in high-speed video, wherein the backface rebounded after the initial primary backface deformation event, and a secondary, smaller, backface deformation was observed. Like the static CT measurements, the depth of the secondary deformation trended opposite to the maximum dynamic deformation. The data indicate that static plate measures currently used to evaluate injury potential may be inadequate, and additional testing and continued analysis should be conducted to gain more information regarding pertinent metrics for BABT injury risk.

Acknowledgments

Funding support for this work was provided by the Army Futures Command Medical Research and Development Command through the Military Operational Medicine Research Program (MOMRP). We would also like to recognise the Army Research Laboratory Weapons and Material Research Directorate, with Dr. Karin Rafaels, for providing insightful experimental input for completing the testing and analysis.

References

[1] Rafaels, K. A., Loftis, K. L., Moholkar, N. M., & Bir, C. A. Comparing the backface deformation behavior between soft and hard body armours. 30th International Symposium on Ballistics. 2017.

[2] Rafaels, K. A., Loftis, K. L., & Bir, C. A. Can clay tell us more than deformation? Personal Armour Systems Symposium, 2018.

[3] Rafaels, K. A., Good, C. H., Loftis, K. L., Satapathy, S. S., Schuster, B. E., Zhang, T. G., McDonald, J. R., et al. Assessment of change in behind-armour blunt trauma (BABT) criteria (ARL-TR-8670). U.S. Army Research Laboratory, 2019.

[4] Cronin, D. S., Bustamante, M. C., Barker, J., Singh, S., Rafaels, K. A., & Bir, C. Assessment of thorax finite element model response for behind armour blunt trauma impact loading using an epidemiological database. Journal of Biomechanical Engineering, 143(3), 2021.

[5] Rafaels, K. A., Choi, K., Glasser, G., & Bir, C. A. Estimation of armour backface velocity. Personal Armour Systems Symposium, 2020.

[6] Lizins, M. E., Matheis, E., Loftis, K. L., & Rafaels, K. Investigating mortality of blunt and penetrating trauma to the torso. Military Health System Research Symposium, 2020.

[7] Rafaels, K. A., Gillich, P. J., & Moholkar, N. M. Importance of areal measurements for thoracic BABT test devices. Personal Armour Systems Symposium, 2016.

[8] Rafaels, K. A., Gillich, P. J., & Moholkar, N. M. Insights into evaluation tools for assessing thoracic behind-armour blunt trauma test devices. 28th International Symposium on Ballistics, 2014.

[9] Bir, C., Rafaels, K., & Loftis, K. Behind armour blunt trauma injuries sustained by law enforcement officers. IRCOBI, 2019.

[10] Bustamante, M., Barker, J., Rafaels, K., Bir, C., Singh, D., Sathananthan, P., & Cronin, D. Shell plate method of reconstructing of behind armour blunt trauma impact scenarios for soft armour using a detailed thorax model. IRCOBI, 2019.

[11] Cronin, D. S., Barker, J., Rafaels, K., & Bir, C. Injury risk assessment for behind armour blunt trauma impact conditions using thorax finite element model. World Congress of Biomechanics, 2018.

[12] Cronin, D., Rafaels, K., Bir, C., Barker, J., Singh, D., Bustamante, M., & Sathananthan, P. Reconstruction of behind armour blunt trauma impact scenarios for soft armour using a detailed thorax model. IRCOBI, 2018.

[13] Rafaels, K., Loftis, K., & Matheis, E. Correlating incoming threats with BABT skin injury. World Congress of Biomechanics, 2018.

[14] Good, C, H., Loftis, K. L., Schuster, B. E., Gillich, P. J., Eberius, N. L., & Ligda, J. P. Re-creation of ballistic impacts to enhanced small-arms protective insert (ESAPI) plates returned from theater (ARL-TR-8439). U.S. Army Research Laboratory, 2018.

[15] Good, C. H., Loftis, K. L., Gillich, P. J., & Eberius, N. L. Analysis of ballistic impacts to hard armour plates returned from theater (ARL-TR-8364). U.S. Army Research Laboratory, 2018.

[16] Loftis, K. L., Good, C. H., Schuster, B. E., & Gillich, P.J. Estimating obliquity of ballistic impacts from residual damage to hard armour plates. Personal Armour Systems Symposium. 2018.

https://doi.org/10.52202/080042-0012